phys. stat. sol. (b) **185**, 137 (1994)

Subject classification: 71.35 and 78.65; 68.55; S8.11; S8.13

Changchun Institute of Physics, Academia Sinica, Changchun[1])

Optical and Structural Properties of ZnTe–ZnS Strained-Layer Superlattices

By

Z. P. GUAN, Y. M. LU, L. C. CHEN, B. J. YANG, and X. W. FAN

ZnTe–ZnS strained-layer superlattices are grown by atmospheric pressure metalorganic chemical vapor deposition on transparent $BaF_2(111)$ and GaAs(100) substrates. With X-ray diffraction measurements, multi-order satellites are observed, which confirms the formation of a periodic structure of the superlattices. Photoluminescence and optical absorption measurements are carried out at 77 K and room temperature. The photoluminescence spectra under different excitations, time-resolved and time-delayed spectra are employed to study the band–band recombination at 77 K. The band structure and strain effects are studied using the uniaxial stress and the linear combination of atomic orbital theory for such high mismatch ZnTe–ZnS strained-layer superlattices. It is noticed that the energy disparity of ZnTe–ZnS superlattices is large with ZnTe or ZnS buffer layers. So the band–band emission can be observed over a wide wavelength region for ZnTe–ZnS superlattices.

1. Introduction

II–VI compound semiconductors producing strained-layer superlattices (SLS) were thought to be particularly promising for optoelectronic devices such as blue color light-emitting diodes (LED), tunable color LEDs, and short wavelength semiconductor lasers. Recently ZnTe–ZnS SLS have been grown by hot wall epitaxy (HWE) [1] and molecular beam epitaxy (MBE) [2, 3]. They all focused on X-ray diffraction, reflective high-energy electron diffraction, and Raman spectroscopy. In most cases, GaAs was used as the substrate material, whose lattice constant ($a = 0.56533$ nm) is in between the lattice constants of ZnTe ($a = 0.61037$ nm) and ZnS ($a = 0.54093$ nm) constituent materials. In the studies of photoluminescence (PL), Fujiyasu et al. and Takeda et al. [4, 5] have reported that they observed strong but rather broad luminescence near 2.6 eV in ZnTe (2.0 nm)–ZnS (5.0 nm) superlattices. However, they did not display the PL spectra of this structure. Teraguchi et al. [6] observed the PL peak around 475 nm at 77 K and considered that the PL peak is due to the deep levels formed in SLS layers due to a large lattice mismatch (13%) between ZnTe and ZnS. In this paper, we first report the emission and absorption processes related to the band–band recombination and study the strained effect of ZnTe–ZnS SLS on GaAs(100) substrates with different buffer layers grown by atmospheric pressure metal-organic chemical vapor deposition (Ap-MOCVD).

2. Experimental

ZnTe–ZnS SLS were grown on $BaF_2(111)$ and GaAs(100) substrates by Ap-MOCVD. The construction of the system has been described in our previous paper [7]. Dimethylzinc

[1]) Changchun 130021, People's Republic of China.

(DMZn), diethyltellurium (DETe), and H_2S were used as the sources of Zn, Te, and S, respectively. DMZn and DETe are controlled in stainless-steel bubblers placed in temperature-controlled baths. High-purity H_2 is used as a carrier gas. The ZnTe–ZnS SLS were grown on fresh natural cleaved faces of BaF_2 single crystals and GaAs substrates; the latter was etched in a solution of 5 H_2SO_4 : 1 H_2O_2 : 1 H_2O for 1 min at 40 °C. After flushing with hydrogen the substrates were heated at 600 °C for 10 min prior to growth in order to desorb volatile species from the surface, then the temperature was reduced to the growth temperature (400 °C). The 337.1 nm line of a N_2 laser with 10 ns duration and 10 Hz frequency was used as the PL excitation source. The PL spectra and time-resolved spectra (TRS) under different excitation densities were detected using a SPEX 1404 double grating spectrometer with a RCA C-31034 cooled photomultiplier. TRS were measured by a Model 440 boxcar.

3. Results and Discussion

3.1 The PL and absorption spectra of SLS

To confirm the presence of the superlattice structure, X-ray diffraction measurements were performed. The measurements were made using an ordinary diffractometer with computer control shown in [8]. Fig. 1 shows the typical PL spectra of the ZnTe (2.8 nm)–ZnS(5.5 nm)/GaAs SLS. It consists of an intense sharp line in the lower energy region and a weaker shoulder in the high energy region; here two peaks are located at 518 nm (band A) and 493 nm (band B) and were observed under high excitation (I_0 = 3 MW/cm^2) at 77 K. This visible luminescence was observed even at room temperature as seen in Fig. 1. The value of the full width at half maximum (FWHM) of the peak at 77 K is 260 meV, which is larger than the values of ZnSe–ZnS SLS and ZnTe–ZnSe SLS. This broadening was caused by: 1. two peaks almost mixed, 2. the fluctuation of the well width and barrier height, and 3. larger mismatch between ZnS and ZnTe (see Section 3.2B).

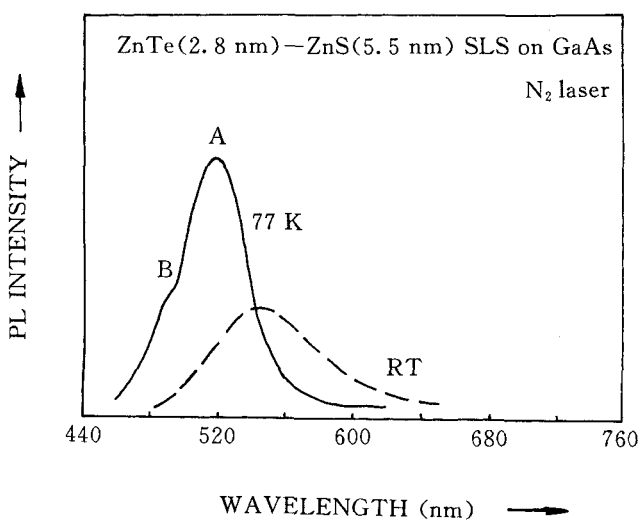

Fig. 1. PL spectra of ZnTe (2.8 nm)–ZnS (5.5 nm) SLS on GaAs substrate at 77 K and room temperature

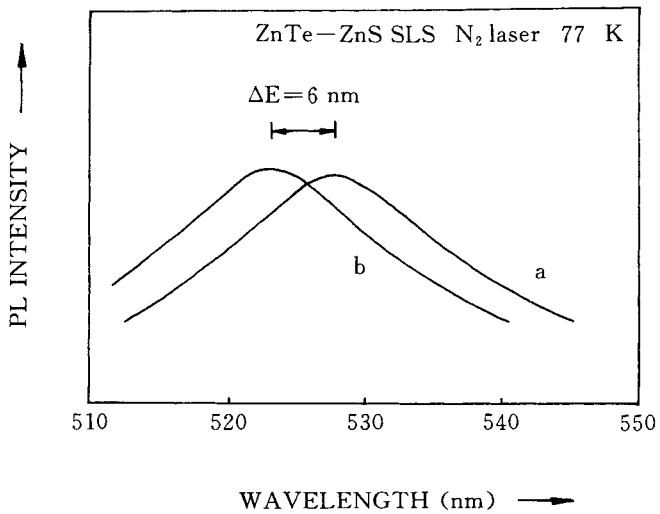

Fig. 2. PL spectra of ZnTe–ZnS SLS on (a) GaAs and (b) BaF_2 substrates with the same growth conditions

ZnTe–ZnS SLS are predicted to be a type-II superlattice system, the allowed subband in this structure can be calculated from the Kronig-Penney band model [9] and strain effect [10]. The PL peaks in ZnTe–ZnS SLS are considered to be related to band–band recombination (see Section 3.3). Fig. 2 shows the PL spectra of ZnTe–ZnS SLS on different substrates with the same growth condition at 77 K. It is noticed that the peak energy position of SLS on the BaF_2 substrate is higher than that of the SLS on the GaAs substrate. The energy disparity is about 6.0 nm. The above samples have the same buffer layer and growth temperature. The energy blue shift is considered to be the quantum size effect due to the layers of ZnS and ZnTe in SLS on

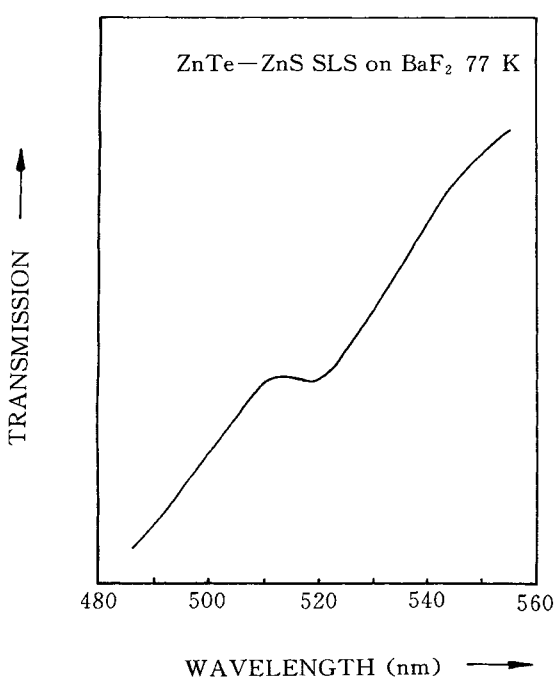

Fig. 3. Absorption spectra of ZnTe–ZnS SLS on BaF_2 with a ZnS buffer layer

BaF_2 being thinner than that of SLS on GaAs substrate. Fig. 3 shows the transmission spectrum of the ZnTe–ZnS/BaF_2 SLS at 77 K. Only one absorption band at 520 nm corresponding to the PL spectra is found. This result indicates that the study of the absorption and bistabilities of ZnTe–ZnS SLS is feasible using this structure.

3.2 PL linewidth and quantum size effect of ZnTe–ZnS SLS

In Fig. 1 the PL peak of the sample is very wide. Besides two peaks mixed, the fluctuation of the well thickness and barrier height and the well width caused by the quantum size effect are playing an important part in the PL spectra of SLS. Using the Kronig-Penney band model, the change of the subband for $n = 1$ electron (in ZnS layer)–hole (in ZnTe layer) is caused by well fluctuation as follows:

$$\Delta E_L = G_S \Delta L_S + G_T \Delta L_T , \tag{1}$$

where

$$G_S = \frac{2E(V_e - E)}{Z_S} [\alpha(\beta^2 - \alpha^2) \sinh(\beta L_T) \cos(\alpha L_S) - 2\alpha^2\beta \cosh(\beta L_T) \sin(\alpha L_S)] , \tag{2}$$

$$\begin{aligned} Z_S = {} & V_e(\alpha^2 + \beta^2) \sinh(\beta L_T) \sin(\alpha L_S) \\ & + [2\alpha\beta^2 L_T E - \alpha(\beta^2 - \alpha^2) L_S(V_e - E)] \sinh(\beta L_T) \cos(\alpha L_S) \\ & + [(\beta^2 - \alpha^2) L_T \beta E + 2\alpha^2 \beta L_S(V_e - E)] \cosh(\beta L_T) \sin(\alpha L_S) , \end{aligned} \tag{3}$$

and

$$\alpha = \frac{\sqrt{2m_S E}}{\hbar} , \tag{4}$$

$$\beta = \frac{\sqrt{2m_T(V_e - E)}}{\hbar} , \tag{5}$$

where G_S and G_T correspond to the electron well of the ZnS conduction band and the hole well of the ZnTe valence band, respectively; m_S, m_T, $V_e = \Delta E_C$ are the electron effective masses of ZnS, ZnTe, and the conduction band discontinuity; L_S and L_T are the thicknesses of ZnS and ZnTe layers. For ZnTe–ZnS wide gap superlattices, dm/dE was ignored in (1) to (3) because of a little change, and the E–L relation was determined by the Kronig-Penney equation [9]. If using $V_h = \Delta E_V$ taking the place of V_e and exchange the position of L_T, m_T in (2) to (5) for L_S, m_S and the electron effective mass with that of hole mass, then G_S becomes G_T. Fig. 4 shows the dependence of the energy difference $\Delta E = (\Delta E_S + \Delta E_T)$ on the well width L for the fluctuation of the well thickness by a monoatomic layer ($\Delta L = 0.27$ to 0.30 nm), here ΔE_S, ΔE_T correspond to ZnS electron well and ZnTe hole well, respectively. In this figure also the pattern of the dependence of ΔE on the barrier height variation as the composition change are given. In the ZnTe–ZnS SLS growth process by Ap-MOCVD, the $ZnTe_{1-x}S_x$ diffusion layer in the ZnTe–ZnS interface, the variation of source temperature and growth temperature would lead to a subband energy change. Using Vegards law [11], in $ZnTe_{1-x}S_x$ layer

$$\Delta V = 1.41 \Delta x \tag{6}$$

and

$$\Delta E_V = (P_S + P_T)\,\Delta V, \tag{7}$$

$$P_S = \frac{E}{Z_S}[(\alpha^2 + \beta^2)\sinh(\beta L_T)\sin(\alpha L_S + \beta L_T(\beta^2 - \alpha^2)\sin(\alpha L_S)\cosh(\beta L_T) + 2\alpha\beta^2 L_T \cos(\alpha L_S)\sinh(\beta L_T)]. \tag{8}$$

Fig. 4a shows the relation $\Delta E_S(\Delta L, L)$ and $\Delta E_S(\Delta V, L)$ for the electron well in the ZnS layer, and Fig. 4b shows the result $\Delta E_T(\Delta L, L)$ and $\Delta E_T(\Delta V, L)$ for the hole well in the ZnTe layer. So the narrower ZnTe layer makes the spectra have a wider peak. ΔE versus Δx is the result of the composition change $\Delta x = 0.1$ at the interface between ZnTe and ZnS layers. Generally the fluctuation of well width and composition is larger than a monoatomic layer especially for Ap-MOCVD. On the other hand, a larger lattice mismatch would lead to an energy disparity based on the different strains at different distances to the face. As we all know, the lattice constants of ZnTe and ZnS layers parallel to the interface have the same value a'' in SLS [12] (see (27) in Section 3.5). In fact, a'' is different at different positions between the inside and outside of the SLS layer. a'' close to the substrate is similar to the lattice constant of the buffer layer, while at the surface of the sample, a'' would be independent of the substrate or buffer layer (see (27)). The uniaxial stress X for each layer is different in the sample, so the energy would change ($\Delta E \sim X$, see Section 3.5). In the calculation it is noticed that the band offsets and the higher lattice mismatch play an important part in the energy shift for II–VI compound wide-gap semiconductor superlattices. For ZnTe–ZnS SLS, $\Delta E_C = 0.49$ eV, $\Delta E_V = 1.9$ eV (see Section 3.5), and misfit $f = 12.8\%$ are much larger than that of many III–V compound superlattices, so the samples have wider PL peaks.

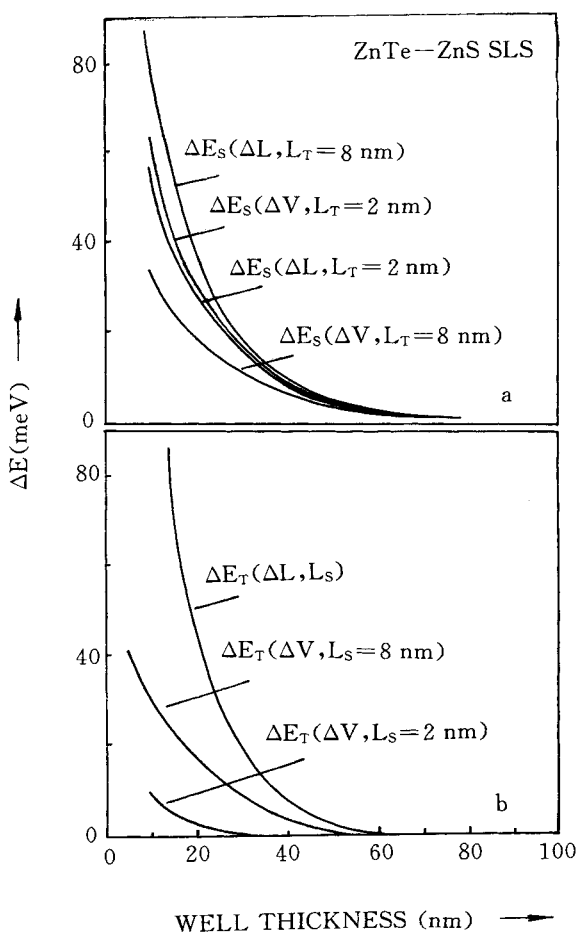

Fig. 4. The dependence of energy change ΔE on the fluctuation of well thickness ΔL ($\Delta L = 0.27$ to 0.30 nm) and barrier height ΔV ($\Delta x = 0.1$) for type-II ZnTe–ZnS SLS. a) ΔE_S in ZnS electron well and b) ΔE_T in ZnTe hole well

3.3 The origin of bands A and B

Fig. 5 shows the excitation density (I) dependence of the PL intensity J and the energy positions of bands A and B at 77 K for ZnTe (2.8 nm)–ZnS (5.5 nm) SLS on GaAs substrate. In relation of $J \sim I^m$, m_A and m_B are about 0.76 and 0.73 in the region of excitation from $0.01I_0$ ($I_0 \sim 3$ MW/cm^2) to I_0. In the above excitation region, the blue shift of the peak amounts to $\Delta E = 80$ meV for band A.

As we all knew, the number of electrons, holes, and excitons increase greatly with increasing excitation. In those cases, the dynamic equation of the above process can be written as

$$\frac{dn}{dt} = I - (A + A')np + K(C + C')n_X^2, \tag{9}$$

$$\frac{dn_X}{dt} = Anp - \frac{n_X}{\tau} - (B + B')nn_X - (C + C')n_X^2, \tag{10}$$

where I is the excitation of electron–hole pair creation [13], $A'np$ describes the radiative or nonradiative direct band–band recombination, Anp corresponds to the creation of excitons, B and B' are the radiative and nonradiative terms of the exciton–electron (Ex–e) scattering process, C and C' are the radiative and nonradiative terms for the exciton–exciton (Ex–Ex) scattering process, n, p, and n_X are the concentrations of electrons, holes, and free excitons, respectively, τ is the lifetime of free excitons, K a constant.

Under dynamic equilibrium $dn/dt = dn_X/dt = 0$ and $n \approx p$, therefore

$$I = (A + A')n^2 - K(C + C')n_X^2, \tag{11}$$

$$An^2 = \frac{n_X}{\tau} + (B + B')nn_X + (C + C')n_X^2. \tag{12}$$

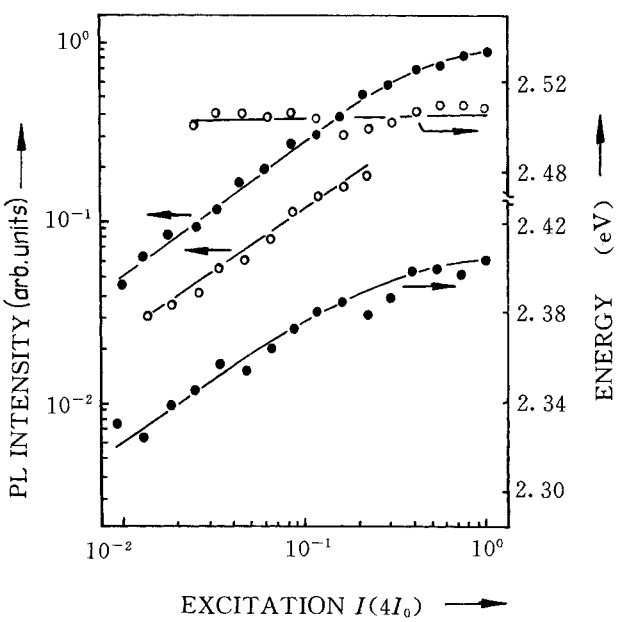

Fig. 5. The excitation density (I) dependence of the PL intensity and energy position of band A (●) and band B (○) at 77 K for ZnTe (2.8 nm)–ZnS (5.5 nm) SLS on GaAs substrate

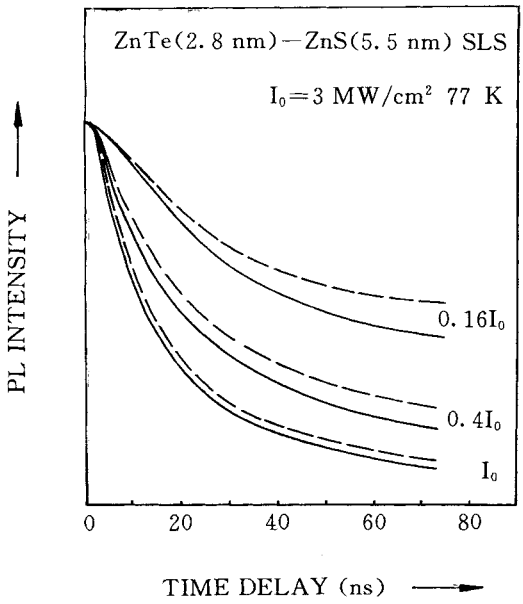

Fig. 6. Time-delayed spectra of ZnTe (2.8 nm)–ZnS (5.5 nm) SLS under different excitations (I_0 = 3 MW/cm²) for band A (———) and band B (– – –)

The free exciton emission, Ex–e scattering, Ex–Ex scattering, and band–band recombination are related to the band edge. Fig. 6 shows the time-delayed luminescence of ZnTe (2.8 nm)–ZnS (5.5 nm) SLS under different excitation with the same features for bands A and B. It is noticed that bands A and B have slower recombination lifetimes and decrease drastically with increasing excitation. The results observed illustrate that the bands A and B are not related to the excitonic emission [14, 15]. In an earlier work [16], we have given the relationship about excitation dependence of the PL intensity at weak, medium, and high excitation. In the three cases, the excitation density is proportional to the PL intensity of the free exciton emission, Ex–e scattering, and Ex–Ex scattering, respectively. For the type-II superlattice system the carrier recombination rate decreases and the lifetime increases due to the different electron and hole wave functions in different layers. The exciton binding energy of type-II superlattices is lower than that of well and barrier materials [17], so the carrier recombination would be dominant and some excitons dissociated under high excitation at 77 K.

For high excitation $(C + C')\, n_X^2$ is dominant and $(C + C')\, n_X^2 \gg n_X/\tau$, it is clear from (11) and (12) that

$$n_X^2 = \frac{(A + A')\, n^2 - I}{K(C + C')} \sim I\,, \tag{13}$$

$$n \sim n_X\,. \tag{14}$$

As we have analyzed above, $A' \ll A$ and band–band recombination $J = An^2 \sim n_X^2$ from (11). Under extremely high excitation the excitons are dissociated and $n_X^2 \sim I^{<1}$. So for band–band emission [22]

$$J \sim I^m \qquad (m < 1)\,. \tag{15}$$

In Fig. 5 $m_A = 0.76$ and $m_B = 0.73$ for bands A and B, respectively, are in agreement with band–band recombination. For $n_X \ll n$ and $A' \ll A$, from (9),

$$J \sim \frac{dn}{dt} = 4I\gamma \frac{\exp(-2\sqrt{IAt})}{[1 - \gamma \exp(-2\sqrt{IAt})]^2} \tag{16}$$

and

$$\gamma = 1 - \frac{2\sqrt{IA}}{n_0\sqrt{A} + \sqrt{I}},$$

where n_0 is the concentration of electrons at $t = 0$ under excitation. The above result with $\tau = 1/2\sqrt{IA}$ is similar with that of [14] a for band–band recombination, indicating that the time constant reduced with excitation increasing. From (11) $I \sim n^2$, it is obtained that the lifetime is inversely proportional to the carrier concentration with $\tau = 1/2n\sqrt{A}$. This result is in agreement with [15] based on the band–band recombination process. Thus, it is reasonable to consider that the PL process of bands A and B are related to the band–band emission, band A and band B were attributed to 1e–1hh and 2e–2hh band–band recombination, respectively.

3.4 Time-resolved spectra

With increasing excitation the peak of band A shifts toward the high-energy side by about 80 meV and band B is almost not changed as seen in Fig. 5. It can be explained by the fact that the number of electrons in the ZnS layer and holes in the ZnTe layer grow and the band filling effect for band A with increasing excitation occurs. For band B corresponding to the high subband (2e–2hh), which has the lower carrier concentration, the effect of band filling is rather weak. In Fig. 6, it is noticed that the disparity of the carrier lifetime between band B and band A $\Delta\tau = \tau_B - \tau_A$ is different at different excitations. The higher the excitation, the less is $\Delta\tau$. That is because the carrier concentration of band B is lower than that of band A and the carrier lifetime is inversely proportional to the carrier concentration. For high excitation, band A shifts toward band B and the spectrum becomes a mixed band. At the energy position of the band B, the carrier of (1e–1hh) the energy level make a contribution to the carrier lifetime, so $\Delta\tau$ decreases gradually with increasing excitation.

Fig. 7 shows the time-resolved spectra of the above sample at 77 K. The peak position of band A at $t = 0$ ns is located at 513.2 nm. As the decay time increases the relative intensity of band A is weaker and the peak shifts toward the lower energy side. After 35 ns the energy shift ΔE is about 52 meV. For the process of measured delay time the peak shift is in the wavelength

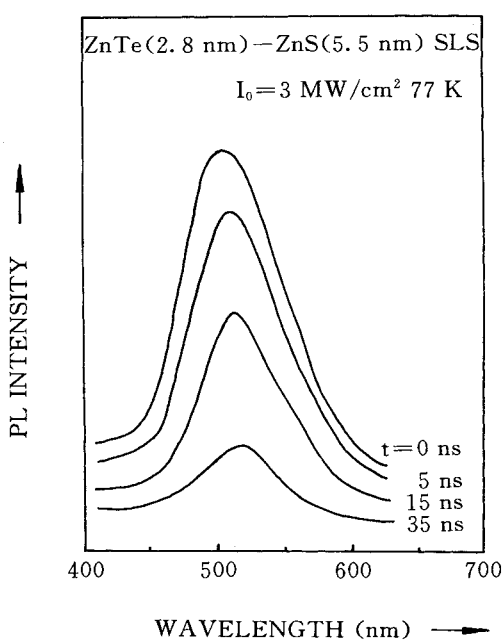

Fig. 7. Time-resolved spectra of ZnTe (2.8 nm)–ZnS (5.5 nm) SLS

region from 513.2 to 530.0 nm, which is in the region of the (1e–1hh) subband. At the early stage of PL decay the carriers with higher energies in band A recombine first. As the time delays the carrier with lower energies recombine then, and the carrier relaxation from the high energy levels to the lower levels lead to the lower energy transition which has the larger lifetime.

3.5 Structure analysis

The band structure of ZnTe–ZnS SLS calculated by the linear combination of atomic orbital (LCAO) approximation [18], the maximum energy ($E_{V\,max}$) at the valence band edge can be calculated as a function of bond length (d, the internuclear distance) as follows:

$$E_{V\,max} = \frac{E_p^c + E_p^a}{2} - \sqrt{\left(\frac{E_p^c - E_p^a}{2}\right) + V_{XX}}, \tag{17}$$

$$V_{XX} = \frac{2 \cdot 16\hbar^2}{m_e^* d^2}, \tag{18}$$

in which E_p^c and E_p^a are the energies of anion and cation atomic P orbital states, V_{XX} is a matrix element between P atomic orbitals, and m_e^* is the effective mass of electrons. The valence-band discontinuity is

$$\Delta E_V = E_{V\,max}^A - E_{V\,max}^B. \tag{19}$$

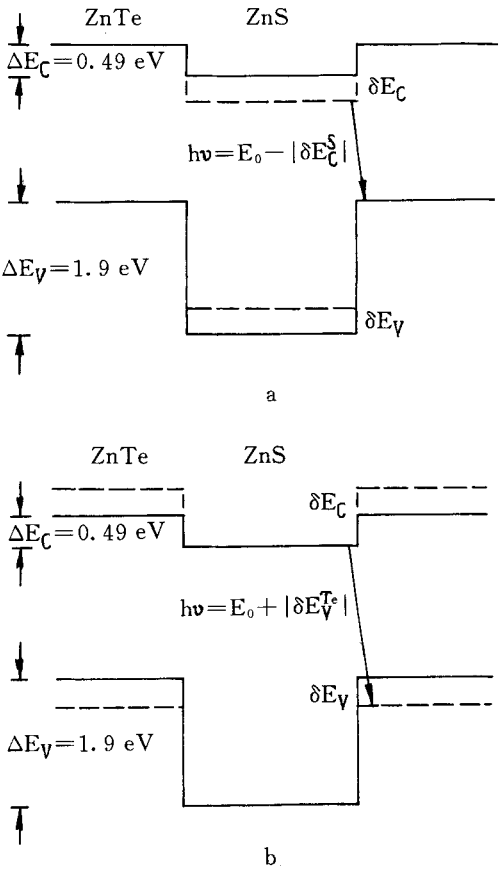

Fig. 8. The band structure of ZnTe–ZnS SLS with a) ZnTe and b) ZnS buffer layer calculated by LCAO theory

Fig. 8 illustrate the energy band structure of ZnTe–ZnS SLS calculated by (17), (18), and (19), the solid line denotes the energy band structure without strain. By selection of different materials as buffer layer, the effective band gap has different values due to the strain effect. The dashed lines in Fig. 8a and b indicate the band structure of ZnTe–ZnS SLS with ZnTe and ZnS buffer layers, respectively. The energy for the band–band transition without strain is

$$E_0 = E_g - \Delta E_V + E_e + E_h + kT, \tag{20}$$

where E_g is the band gap of ZnS single crystal, E_e and E_h are the electronic energy

levels in ZnS conduction band and the hole energy level in ZnTe valence band, kT is the kinetic energy of the electrons or holes in ZnTe–ZnS SLS. At strain the conduction and valence bands shift due to the hydrostatic pressure component of the strain, an effect described by the deformation potentials for the conduction (a_C) and valence (a_V) bands, and $a = a_C - a_V$ [19]. For uniaxial stress X parallel to the [001] direction ($X \parallel [001]$), the band gap shift can be written as

$$\begin{aligned}\delta E_g &= \delta E_C + \delta E_V \\ &= 2a(S_{11} + 2S_{12})X - b(S_{11} - S_{12})X \\ &= 2a_C(S_{11} + 2S_{12})X - 2a_V(S_{11} + 2S_{12})X - b(S_{11} - S_{12})X,\end{aligned} \tag{21}$$

where S_{ij} are the elastic compliance constants, b is the shear deformation potential of the valence band. If using ZnTe as buffer layer above 1.0 μm the lattice constant of ZnTe in SLS layer is almost not changed comparing with its single crystal value, while both layers of ZnTe–ZnS SLS are thin enough. Then a tensile strain acts in the ZnS layer, the energy gap will decrease. The energy shift of the conduction band for ZnS is

$$\delta E_C^S = 2a_C(S_{11} + 2S_{12})X \tag{22}$$

and

$$X = \frac{(a'' - a_0)}{a_0} \frac{1}{S_{11} + S_{12}}, \tag{23}$$

where a'', a_0 are, respectively, the lattice parameters of the ZnS with in-plane strain and without strain. It is assummed that the well and barrier thicknesses are not changed. Under the effect of strain the band–band transition of SLS with ZnTe buffer layer is

$$h\nu = E_0 - |\delta E_C^S|. \tag{24}$$

So the energy transition will shift towards the low energy side as seen in Fig. 8a. On the contrary, using ZnS as buffer layer a compressive strain is introduced in the ZnTe layer.

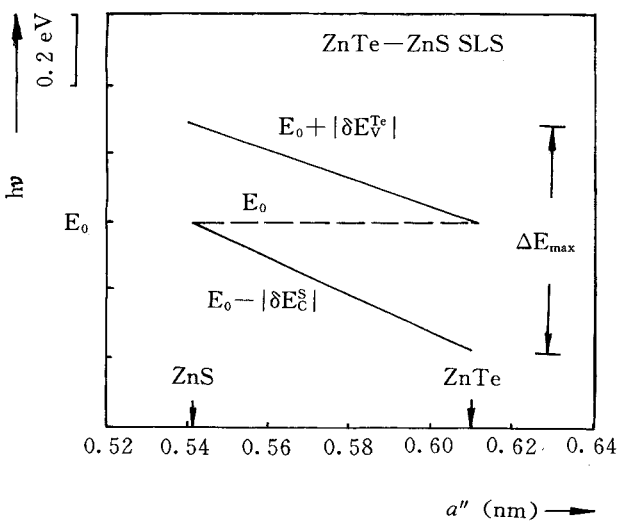

Fig. 9. Variation of $h\nu$ as a function of a''

Table 1
The parameters of ZnTe and ZnS used in the text

parameter	ZnS	ZnTe
a_C (eV)	− 4.09 [19]	−2.70 [20]
a_V (eV)	2.31 [19]	1.35 [20]
b (eV)	− 1.25 [19]	−1.78 [20]
S_{11} (10^{-11} m^2/N)	1.839 [21]	2.40 [21]
S_{12} (10^{-11} m^2/N)	− 0.707 [21]	−0.873 [21]
E_g (eV)	3.80 [18]	2.39 [18]
E_V (eV)	−11.40 [18]	−9.50 [18]
a_0 (nm)	0.54093	0.61037

The ZnTe energy gap will increase and the transition energy of SLS will increase (Fig. 8b). The valence band shift of ZnTe is

$$\delta E_V^{Te} = -2a_V(S_{11} + 2S_{12})\,X - b(S_{11} - S_{12})\,X \tag{25}$$

and the band–band transition is

$$h\nu = E_0 + |\delta E_V^{Te}|\,. \tag{26}$$

Fig. 9 shows the change range of the band–band transition in ZnTe–ZnS SLS with ZnS or ZnTe buffer layer due to the strain, respectively. The parameters of ZnTe and ZnS used in the calculations are listed in Table 1. The lattice constants of ZnTe and ZnS layers parallel to the interface have the same value in SLS. As a result, the average lattice constant a'' [12] is given by

$$a'' = \frac{(a_{ZnS}G_{ZnS}h_{ZnS} + a_{ZnTe}G_{ZnTe}h_{ZnTe})}{(G_{ZnS}h_{ZnS} + G_{ZnTe}h_{ZnTe})}, \tag{27}$$

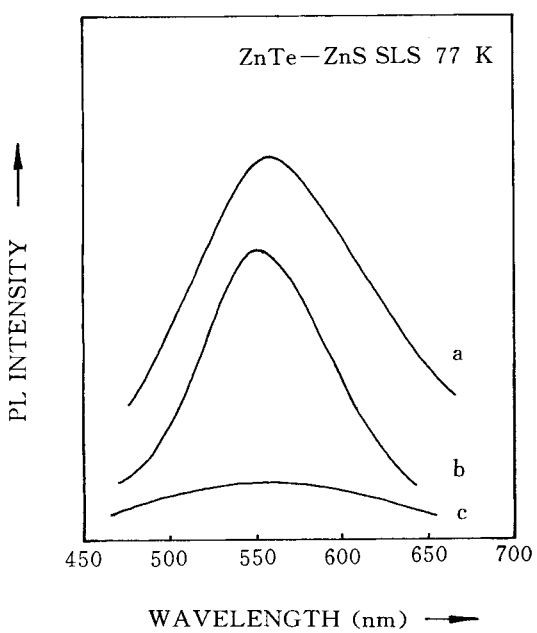

where a_{ZnTe}, a_{ZnS} are the stress-free lattice constants for ZnTe and ZnS, G_i are the shear moduli, h_{ZnTe} and h_{ZnS} are layer thicknesses of ZnTe and ZnS in ZnTe–ZnS SLS, respectively. The value of a'' is between the lattice constants of ZnTe and ZnS. In order to get the different energy transitions of ZnTe–ZnS SLS, we can select different buffer layers

Fig. 10. PL spectra (77 K) of ZnTe–ZnS SLS at the same growth conditions (the growth times for ZnTe and ZnS layers are 7 and 30 s, respectively) on GaAs substrate (a) without buffer layer, (b) with ZnS, and (c) with ZnTe buffer layer

or no buffer layer to grow ZnTe–ZnS SLS. As the lattice mismatch of ZnTe–ZnS SLS is about 13%, the shift of $h\nu$ is larger as seen in Fig. 9. The energy change $\Delta E_{\max} = |\delta E_V^{Te}| + |\delta E_C^S|$ in ZnTe–ZnS is about 0.7 eV nearby E_0.

Fig. 10 shows the spectra of ZnTe–ZnS SLS at the same growth conditions (the growth times for ZnTe and ZnS layers are 7 and 30 s, respectively) with different buffer layers. It is noticed that the peak energy of the SLS with the ZnS buffer layer is situated at higher energy than that of the sample without a buffer layer. This difference is considered to be due to the strain effect as the above analysis shows. If the ZnS layer is rather thick, a'' is close to the lattice parameter of ZnS, so the peak of SLS on ZnS buffer layer has the narrower FWHM than that of SLS on GaAs without a buffer layer, and the mismatch between a'' and the ZnTe buffer layer is large. In the ZnS layer of SLS many kinds of dislocations and defects occur. So the sample has a bad crystal quality.

4. Conclusion

1. We reported on the successful growth process of ZnTe–ZnS SLS on GaAs and BaF_2 substrates with different buffer layers by Ap-MOCVD.

2. It is observed for the first time that the emission and absorption are related to the band–band recombination in ZnTe–ZnS SLS on the BaF_2 substrate at 77 K. We also observed the emission of ZnTe–ZnS SLS on GaAs substrate at 77 K and room temperature, indicating a sample of good quality.

3. At the same growth condition the growth rate of ZnTe–ZnS SLS on BaF_2 (111) is slower than that of ZnTe–ZnS SLS on GaAs(100) substrate, so the PL peak of ZnTe–ZnS SLS on BaF_2 is higher.

4. It is analyzed that the PL linewidth ΔE depends on the fluctuation of the well thickness ΔL, barrier height ΔV and an uneven strain in SLS layer. We think that larger band offsets, higher lattice mismatch, and excess carrier effect play an important part in the FWHM of band–band recombination for II–VI compound superlattices.

5. Using the PL spectra under different excitation, the time-resolved and time-delayed spectra of the bands A and B are attributed to the band–band recombination of the (1e–1hh) and (2e–2hh) subbands, respectively.

6. It is considered that using different buffer layers the band–band transitions of SLS have different values due to the strain effect.

Acknowledgements

This work was supported by the High Technology Research Programs in China and the Great National Natural Science Foundation of China, and the project was supported by Laboratory of Excited State Processes, Changchun Institute of Physics, Chinese Academy of Sciences. We could like to thank Mr. Y. C. Liu for his discussion.

References

[1] L. H. SHON, K. INOUE, K. MURASE, H. FUJIYASU, and Y. YAMAZAKI, Solid State Commun. **62**, 621 (1987).
[2] T. KARASAWA, K. OHKAWA, and T. MITSUYU, Appl. Phys. Letters **54**, 117 (1989).
[3] T. KARASAWA, K. OHKAWA, and T. MITSUYU, J. appl. Phys. **68**, 4581 (1990).
[4] H. FUJIYASU, K. MOCHIZUKI, Y. YAMAZAKI, M. AOKI, and A. SASAKI, Surface Sci. **174**, 543 (1986).

[5] T. Takeda, T. Kurosu, M. Lida, and T. Yao, Surface Sci. **174**, 548 (1986).
[6] N. Teraguchi, Y. Takemura, R. Kimura, M. Konagai, and K. Takahashi, J. Crystal Growth **93**, 720 (1988).
[7] G. H. Fan, J. I. Davies, and J. O. Williams, Chin. J. Lum. **7**, 384 (1987).
[8] Z. P. Guan, Y. M. Lu, B. J. Yang, and X. W. Fan, Superlattices and Microstructures **13**, 101 (1993).
[9] R. Kronig and W. G. Penney, Proc. Roy. Soc. A **130**, 499 (1931).
[10] H. Mariette, F. Dalbo, N. Magrnea, G. Lentz, and H. Tuffigo, Phys. Rev. B **38**, 12443 (1988).
[11] E. Kasper, Surface Sci. **174**, 630 (1986).
[12] C. G. Van de Wall and R. M. Martin, Phys. Rev. B **34**, 5622 (1986).
[13] C. B. a la Guillaume, J. M. Debever, and F. Salvan, Phys. Rev. **177**, 567 (1969).
[14] J. Christen and D. Bimberg, Surface Sci. **174**, 261 (1986).
[15] Y. H. Sakaki, M. Nishioka, and H. Yoshino, Appl. Phys. Letters **46**, 519 (1985).
[16] Z. P. Guan, Z. H. Zheng, J. H. Zhang, Y. M. Lu, G. H. Fan, and X. W. Fan, phys. stat. sol. (b) **169**, 339 (1992).
[17] H. Yang, A. Ishida, H. Fujiyasu, and H. Kuwabara, J. appl. Phys. **65**, 2838 (1989).
[18] W. A. Harrison, J. Vacuum Sci. Technol. **14**, 1016 (1977).
[19] K. Shahzad, D. J. Olego, C. G. Van de Wall, and D. A. Cammack, J. Lum. **46**, 109 (1990).
[20] R. H. Miles, G. Y. Wu, M. B. Johnson, T. C. McGill, J. P. Faurie, and S. Sivanatthan, Appl. Phys. Letters **48**, 1383 (1986).
[21] D. Berlincurt, H. Jaffe, and L. R. Shiozawa, Phys. Rev. **129**, 1009 (1963).
[22] A. Opanowicz, K. Marinova, H. Liebing, and W. Ruppel, phys. stat. sol. (b) **75**, 471 (1976).

(Received March 21, 1994; in revised form June 22, 1994)